



# Mechanical, viscoelastic and sorption behaviour of acrylonitrile–butadiene–styrene composites with 0D and 1D nanofillers

N. Rasana<sup>1,2</sup> · K. Jayanarayanan<sup>1,2</sup> · Alessandro Pegoretti<sup>3</sup> · G. Rammanoj<sup>1</sup> · K. Arunkumar<sup>1</sup> · T. Hariprasanth<sup>1</sup>

Received: 9 March 2021 / Revised: 20 August 2021 / Accepted: 14 September 2021 /  
Published online: 26 September 2021

© The Author(s), under exclusive licence to Springer-Verlag GmbH Germany, part of Springer Nature 2021

## Abstract

This work presents an investigation on the morphology, mechanical, viscoelastic and transport properties of acrylonitrile–butadiene–styrene (ABS) nanocomposites reinforced with nanosilica (NS) and multiwalled carbon nanotubes (MWCNTs). The nanofillers content was varied from 1 to 5 wt%. Morphological and mechanical investigations revealed a better dispersion and effective stress transfer in carboxyl-treated MWCNT composites with respect to silane-treated NS. The highest values of tensile strength and Young's modulus were reached for 5 wt% of MWCNT. Theoretical modelling of elastic modulus of the composites with carbon nanotubes (CNT) was in good agreement with experimental data. On the other hand, in the case of composites with NS an interfacial modulus of 2.5 GPa was assumed in the model to approach the experimental data. The highest value of storage modulus was reported at a MWCNT content of 5 wt% followed by 3 wt% which discloses the stiffening effect of long curly CNTs in comparison with NS. The damping behaviour indicated a lowering and broadening of  $\tan \delta$  peak induced by CNT. The storage modulus and damping behaviour of the nanocomposites were analysed using theoretical models in which aspect ratio, stiffening effect, adhesion and entanglement phenomena were included. The lowest solvent diffusivity and permeability was exhibited by composite with MWCNT at 5 wt% owing to the tortuosity, higher adhesion and aspect ratio of the filler and revealed a decrement in permeability by 62% with regard to neat ABS.

**Keywords** Acrylonitrile–butadiene–styrene · MWCNT · Nanosilica · DMA · Diffusivity · Damping

---

✉ N. Rasana  
n\_rasana@cb.amrita.edu; rasana9@gmail.com

Extended author information available on the last page of the article

## Introduction

Acrylonitrile–butadiene–styrene terpolymer (ABS) is one of the main polymers in the styrene family, and its properties depend on the content of the three major constituents (acrylonitrile, butadiene and styrene). The heat stability and chemical resistance are contributed by the acrylonitrile phase, rigidity and processability by the styrene phase, and the impact strength and toughness being provided by butadiene, the rubbery phase [1, 2]. These properties could be further enhanced by the incorporation of suitable nano-fillers, and the obtained nanocomposites have demonstrated superior properties over microcomposites and conventional materials. Recent studies [3–5] have proven that even limited content of filler (up to 5 wt%) can significantly enhance the mechanical, thermal, barrier, electrical properties, etc., with respect to conventional microcomposites which require higher loading of microfillers to achieve similar performances. Improved properties in nanocomposites can be reached when a consistent dispersion and distribution of fillers in the polymer matrix is reached [3]. Different types of organic and inorganic fillers like aluminium oxide ( $\text{Al}_2\text{O}_3$ ) [4–8] zinc oxide (ZnO) [9, 10] carbon nanotubes [11–13] nanoclay [14], halloysite nanotubes [15], graphene [16] were used to improve the properties of polymer matrices.

Several studies have been reported on ABS reinforced with nanofillers. Gao et al. [17] synthesized ABS/reduced graphene nanocomposites (rGO) and utilized the advantages of ABS matrix, like chemical resistance, heat resistance, recyclability and ease of processing along with conductive characteristics of graphene sheet. The resultant ABS/rGO composite demonstrated excellent electrical conductivity, thermal conductivity and improved mechanical properties. ABS/graphene oxide (GO) nanocomposites with carboxyl and hydroxyl surface functional groups attached on filler and at a loading less than 0.1 wt% have been developed for 3D printing applications by Brennan et al. [18]. The authors reported that GO could enhance the tensile strength, elongation at break and toughness and could maintain the stiffness which is suitable for various applications of static and dynamic loadings. Dynamic mechanical parameters of MWCNTs/ABS composites and their correlation with entanglement density of polymer chains and the dispersion effectiveness were explained by Abraham et al. [19]. Another work evaluated the electromagnetic shielding effectiveness of ABS/reinforced with carbonaceous fillers like carbon black and carbon nanotubes [20]. ABS-reinforced nanosilica composites were prepared by Kyratsis et al. [21] to investigate its applicability in 3D printed structures and reported that incorporation of nanosilica enhanced the stiffness and hardness particularly for 10 wt% content [21]. Some of the earlier works have reported the property enhancement of ABS composites reinforced with nanosilica [21–23] and CNT fillers [24–27].

This work is focused on the melt compounding and characterization of nanosilica and MWCNT-reinforced ABS composites. In order to ensure the better effectiveness of filler dispersion, surface treatment of nanosilica was performed using silane and MWCNTs with carboxyl groups. The bonding mechanism of fillers with ABS matrix was elucidated and an analysis of the variation in tensile

strength, modulus and impact strength was conducted. The theoretical modelling of modulus of 0D (nanosilica) and 1D (MWCNT)-reinforced ABS composites using Cox and Ji models based on the interfacial characteristics and L/D ratios of the nanofillers have been conducted. The variation in storage and damping parameter with respect to temperature was studied using dynamic mechanical analysis, and the effect of two types of filler reinforcements on stiffening effect at glassy plateau and relaxation of polymer chains at glass transition region ( $T_g$ ) was examined. Theoretical models were used to predict the storage modulus damping factor and the effect of localized constrained phases. The transport properties like permeability, diffusivity and sorption coefficient were evaluated for a suitable permeant, toluene. The trend in the diffusivity was measured at successive time intervals and is correlated with reduction in free volume, adhesion and interactions of fillers with the matrix.

## Experimental and characterization methods

The base matrix used was acrylonitrile–butadiene–styrene (melt flow index of 4.4 gm/10 min) which was provided by Reliance Industries, India. Nanosilica ( $\text{SiO}_2$ ) was provided by Nanowings Pvt. Ltd, India, with an average primary particle size lower than 100 nm. Surface treatment of nanosilica was accomplished with 3-amino propyl tri ethoxy silane. MWCNTs (Specific surface area: 210  $\text{m}^2/\text{g}$ ) was supplied from United Nanotech Innovations Pvt. Ltd with an average diameter of 20–30 nm and length of 10–20  $\mu\text{m}$ . MWCNT was treated with 1.5 wt% of carboxylic acid. ABS-g-MAH (20 g in 500 g batch) compatibilizer was used to enhance the dispersion of nanofillers (MWCNTs and nanosilica) in ABS matrix.

Masterbatches of nanosilica and MWCNT nanofillers in ABS matrix were prepared using a laboratory-scale internal mixer of capacity 40 g. The concentration of MWCNT or nanosilica was at 12.5 wt% in the masterbatches. The mixer was equipped with heating coils, and temperature in the chamber was set at 200 °C. The rotor blade speed was set at 30 rpm, and the masterbatches of MWCNT and nanosilica in ABS polymer were prepared and then granulated. The melt compounding of the required quantity of masterbatch and ABS was carried out in a co-rotating twin screw extruder with screw length to diameter ratio of 30:1 and at a screw speed of 100 rpm. During compounding, 4 wt% of ABS-g-MAH was added at regular time intervals to the feeder zone of the extruder. The extruded melt in the form of strands emerging from the die was cooled in a waterbath and solidified. The processing temperatures in the extruder were maintained at 160 °C, 190 °C, 210 °C and 250 °C from feed to die zone, respectively. The cooled strands pulled out from the waterbath were pelletized and then injection moulded (Ferromatik Milacron Sigma 50 T) to dumbbell-shaped tensile test specimens according to ASTM D638. The specimen codes and the nanofiller content in the composites are reported in Table 1. The composite is designated as A, AN and AC composites. A represents ABS, AN and AC composites refer to nanosilica and carbon nanotube-reinforced composites, respectively, with nanofiller content varying from 1, 3 and 5 wt%. AF represents the ABS matrix functionalized with 4 wt% ABS-g-MAH (Table 2).

**Table 1** Specimen nomenclature and the content of nanofiller, compatibilizer and ABS in each composite

Sample code	ABS (g)	Nanosilica (g)	MWCNTs (g)	ABS-g-MAH (g)	Total weight of each sample (g)
A	500	0	0	0	500
AF	480	0	0	20	500
AN1	475	5	0	20	500
AN3	465	15	0	20	500
AN5	455	25	0	20	500
AC1	475	0	5	20	500
AC3	465	0	15	20	500
AC5	455	0	25	20	500

**Table 2** Impact strength of ABS-reinforced nanosilica and CNT composites

Specimen	Impact strength (J/m)
A	321
AF	150
AN1	164
AN3	159
AN5	136
AC1	146
AC3	154
AC5	157

The morphology of the composite was revealed with a scanning electron microscope JEOL JSM 6490 LA SEM. The square samples of size 0.5 cm were sputtered with 2 nm thickness of gold–palladium layer for the analysis. Transmission electron microscopy Jeol/JEM 2100 TEM was used to reveal the nanofiller dispersion in the matrix. Ultra-thin slices of composite specimen were prepared using an ultramicrotome and placed on Cu grid mesh for analysis. The mechanical properties of the composites were investigated using an universal tensile testing machine (Tinius Olsen) with a constant cross-head speed of 50 mm/min on ASTM D638 dumbbell-shaped test specimens at room temperature. Dynamic mechanical analysis (DMA) technique was used to characterize the viscoelastic behaviour of the composites. DMA was performed by a PerkinElmer DMA800 in dual cantilever mode in the temperature range from 30 °C to 200 °C scanned at a heating rate of 5 °C/min at a frequency of 1 Hz and a maximum strain of 0.02%. Rectangular specimens of length 43 mm, width 13.2 mm and thickness 3.3 mm were tested. Notched izod impact strength test was performed using Instron 9050 equipment according to ASTM D256 standard. Six specimens were tested, and the average values were reported with standard deviations. For sorption test, square

samples of size  $20 \times 20 \text{ mm}^2$  were prepared and the outer edges were rounded off to enable uniform absorption of the solvent from all directions. The thickness of all the samples was maintained as 3 mm. The samples were dipped completely in the solvent (toluene) and at different time intervals they were taken out and the excess solvent was removed with a filter paper. The samples were then weighed, and the procedure was repeated until solvent sorption reached equilibrium.

## Results and discussion

### Microstructure development

The microstructure of the composites was analysed using scanning and transmission electron microscopy (SEM and TEM). At 3 wt% of nanosilica content in ABS matrix, the dispersion of nanosilica was consistent which could be revealed from the SEM and TEM micrographs (Figs. 1a–c and 2a), respectively. In Fig. 1a–c, the SEM micrographs of AN3 composites, dispersed nanosilica could be observed as white spherical particles. Whereas, in the case of MWCNT reinforced composites better dispersion and distribution of MWCNTs could be observed at nanotube content of 5 wt% in comparison with nanosilica-reinforced composites. The SEM micrographs of AC5 composites (Fig. 1d–f) at higher magnification clearly reveal the uniform dispersion of MWCNTs which could be observed as white curly lines and projections in the images. Furthermore, agglomerates of the nanofillers were visible at 3 wt% nanosilica.

The TEM image of AN3 composite (Fig. 2a) reveals the inconsistent distribution and the existence of agglomerates relative to 5 wt% nanotube-reinforced ABS composite (Fig. 2b). A complicated 3D network of MWCNTs can be seen in Fig. 2a which proves that at 5 wt% loading nanotubes creates sufficient contacts between them to generate a percolated network within ABS. As evidenced in Fig. 2a, at higher content of MWCNTs the inter-particle distance reduces which establish the conditions for the development of a firm interfacial layer via the carboxyl (–COOH) treatment of MWCNTs.

Furthermore, an enhanced interfacial adhesion could be generated due to the strong hydrogen bonding of anhydride groups on the compatibilizer with carboxyl groups on the MWCNTs. Moreover, excellent dispersion and strong interface could be noticed in TEM micrographs of AC5 composite owing to the compatibility between the styrene–acrylonitrile polar groups on the ABS matrix and the MWCNTs. Conclusively, the micrographs indicate that carboxylic acid-treated MWCNT was dispersed in ABS composites more effectively than silane-treated nanosilica in the presence of maleic anhydride compatibilizer. Dul et al. [27] reported the microstructure of ABS/CNT nanocomposites prepared via two step (mixing in an internal mixer and further extruded in twin screw) melt mixing process. The authors described the uniform dispersion of CNTs in ABS matrix and pointed out the limited presence of nanoaggregates owing to the two step method adopted for the preparation of test specimens. Their findings are in good

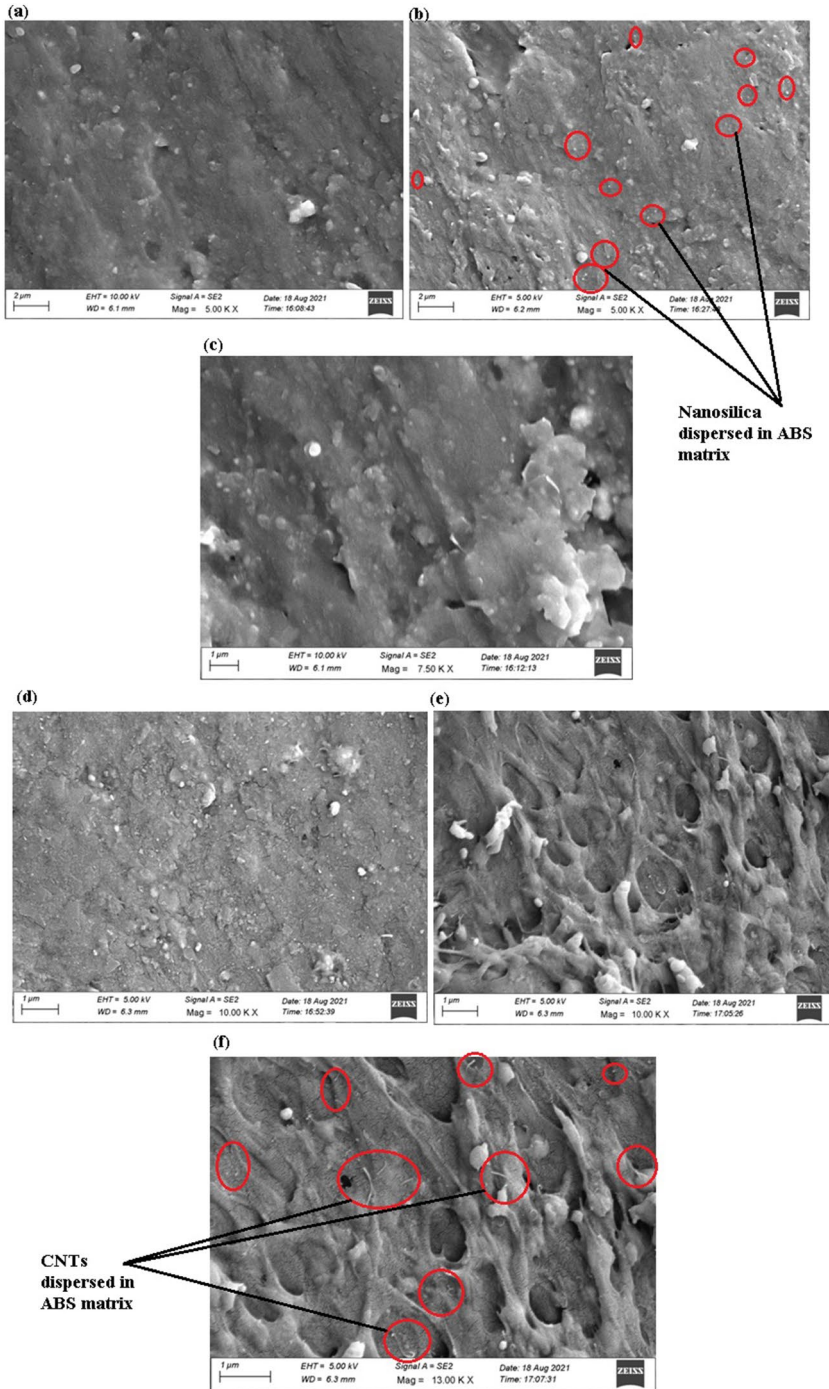


**Fig. 1** SEM micrographs of (a–c) AN3 composite showing the dispersion of nanosilica in ABS matrix (d–f) AC5 composite showing the dispersion of MWCNTs in the ABS matrix at increasing magnifications

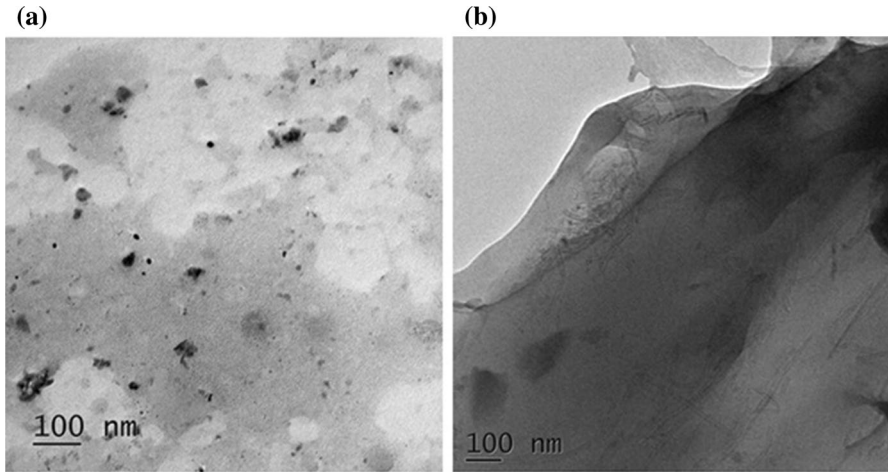


**Fig. 2** TEM micrographs of **a** AN3 composite showing the dispersion of nanosilica **b** AC5 composite showing the dispersion of MWCNTs in the ABS matrix

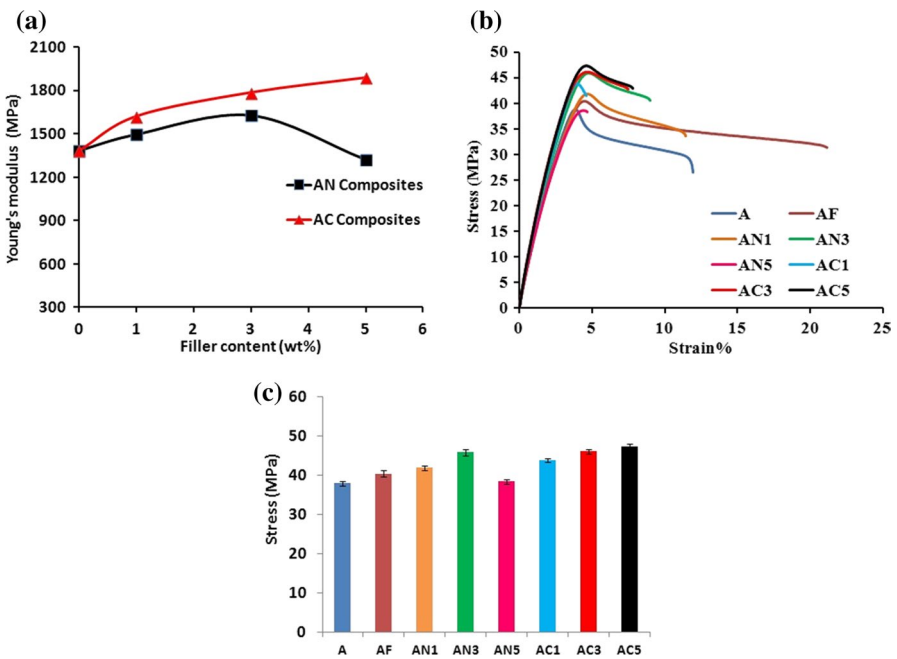


**Fig. 3** **a** Young's modulus variation with filler content **b** Stress vs strain curves of CNT as a function of the filler content **c** Ultimate tensile strength of composites with error bars

agreement with the SEM micrographs reported in the current study, and at higher magnifications large number of well distributed CNTs were observed leading to better adhesion between the ABS and CNTs. The dispersion levels of CNTs in ABS matrix at varying concentrations (1, 5 and 10 wt%) were also discussed by Sahil et al. [28]. Excellent dispersion at 5 wt% of CNTs and dense agglomerations beyond 5 wt% was revealed in their study.

### Static mechanical properties

The tensile properties of virgin ABS and the various investigated nanocomposites are reported in Fig. 3. As indicated in Fig. 3a, the presence of MWCNT whose content was varied from 1, 3 and 5 wt% shows a positive effect on the Young's modulus.

It could be noted that for nanosilica-reinforced composites at 3 wt% filler content the Young's modulus and tensile strength were 1629 MPa and 45.87 MPa, respectively, and beyond 3 wt% the modulus decreases. This decrement could be attributed to the presence of agglomerates of nanosilica at its higher content (which was also confirmed by SEM and TEM analysis). In addition, 1 and 3 wt% of nanosilica-reinforced composite manifested a semi-ductile fracture relative to CNT-reinforced ABS composites which results in strain at break values of 11.45% and 8.9%, respectively. In the case of AF sample, the addition of ABS-g-MAH could enhance the interaction and adhesion between the polymer chains that raised the tensile strength. Further, the higher strain percentage could be attributed to the stick and slip condition of polymer chains in the presence of compatibilizer. Amongst ABS/nanosilica (AN) composites, rupture strength was maximum for AN3 composite and at higher content (5 wt%) of nanosilica, rupture strength was minimal with lowest strain at break owing to the formation of crazes through stress concentrations. The rupture strength and yielding is low in AC1 composite, due to the insufficient amount of CNTs to entangle with polymer chains. The AC5 composite exhibits higher rupture strength but relatively brittle failure with regard to nanosilica composites owing to their higher stiffness. The effective stress transfer takes place and hence, the load the composite can take up before failure improves. The highest tensile strength (47.3 MPa) among the investigated materials was reported by AC5 composite which is 21.8% higher than the virgin ABS (A). From Fig. 3a, an increasing trend in modulus can be observed with increasing filler content for ABS/CNT composites. A Young's modulus of 1890 MPa was reported for AC5 composite with elongation at break of 7.6%. These findings conform well with the trend observed in tensile properties of ABS/CNT composites reported by Dul et al. [27]. The authors clearly described that the tensile modulus and yield strength enhanced with the inclusion of CNTs. They reported an increment in tensile modulus by 19% at nanotube content of 8 wt% with respect to virgin ABS, whereas in the present study elastic modulus enhanced by 36.4% at 5 wt% MWCNT with regard to neat ABS. In another study, authors [29] explained the constrained butadiene phase in the presence of CNTs as one of the causes for the enhanced tensile modulus and strength of ABS/CNT composites. Sahil et al. [28] also reported an increasing trend in Young's modulus till 5 wt% of MWCNTs in ABS matrix. The well dispersed and distributed CNTs in

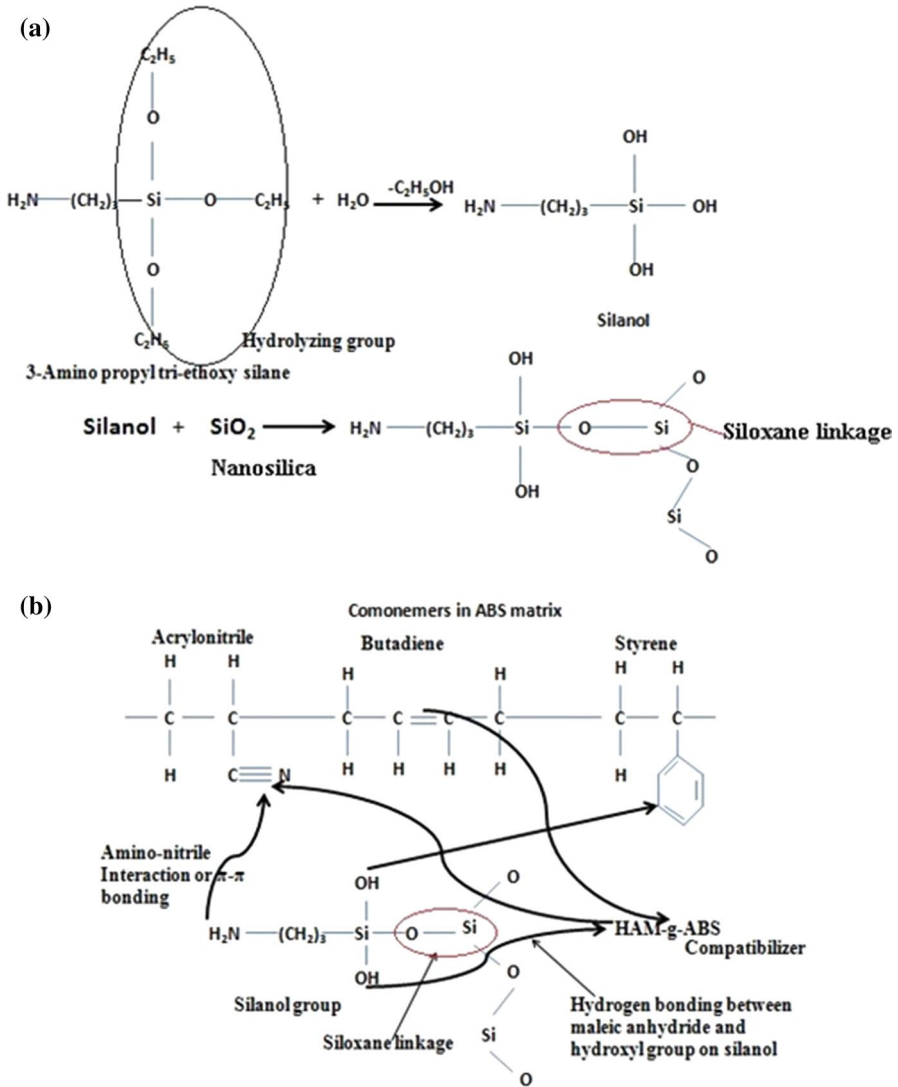


**Fig. 4** a Silanization of nanosilica with silanol obtained by hydrolysis of 3-amino propyl triethoxy silane (3-APTES) b Bonding mechanism of silane-treated nanosilica in the presence of ABS-g-MAH compatibilizer with comonomers of ABS matrix

ABS matrix (as observed in micrographs) and the long curly geometry of MWCNTs could adhere and entangle well with butadiene phase and restrict the mobility and amplifies the energy absorption capability of AC5 composite.

## Mechanism of bonding

Amongst the nanosilica-reinforced ABS composites, better mechanical properties were reported at 3 wt% nanofiller and the possible reaction mechanism (Fig. 4) and bonding which offers higher interfacial adhesion is due to the following facts. Nanosilica was treated with 3-aminopropyl triethoxy silane coupling agent before processing (Fig. 4a). The purpose of this silane surface treatment along with the addition of ABS-g-MAH compatibilizer is to ensure the effective dispersion of nanosilica within the ABS matrix through the formation of silanol group and strong siloxane bonding [30]. Furthermore, strong hydrogen bonding could occur with the hydroxyl groups present on the silica surface and styrene groups present on ABS (Fig. 4b).

ABS-g-MAH added with MWCNTs in ABS matrix promotes the finer dispersion of fillers in the matrix.

The surface treatment of MWCNTs with carboxylic acid groups causes the strong hydrogen bonding with maleic anhydride group on ABS-g-MAH which leads to higher dispersion of nanotubes (Fig. 5). Furthermore, in comparison with nanosilica, larger ( $l/d$ ) ratio of MWCNTs enhances the contact surface between the filler and the matrix improving the interfacial interaction and the stiffening effect [31]. In comparison with silane-treated nanosilica, carboxyl-treated MWCNTs promote better dispersion and effective stress transfer which is the reason of the improved tensile strength and modulus [32].

## Micromechanical modelling of modulus of the composites

The Young's modulus of the nanosilica-reinforced ABS composites was theoretically evaluated using the model proposed by Ji et al. [33]. This three phases model considers the matrix, the filler and the interfacial characteristics to predict the Young's modulus ( $E_c$ ) of composites reinforced with spherically shaped nanoparticles. The Ji model is expressed by the following set of Eq. (1).

$$E_c = E_m \left[ (1 - \lambda) + \left( \frac{\lambda - \beta}{(1 - \lambda) + \frac{\lambda(k-1)}{\ln k}} \right) + \frac{\beta}{(1 - \lambda) + \frac{(\lambda - \beta)(k+1)}{2} + \beta \frac{E_f}{E_m}} \right] \quad (1)$$

where

$$\lambda = \sqrt{\left( \frac{r_i + r_f}{r_f} \right)^3 \varphi_f} \quad ; \quad \beta = \sqrt{\varphi_f} \quad \text{and} \quad k = \frac{E_i}{E_m} \quad (1(a), (b), (c))$$

The parameters  $r_i$  and  $r_f$  represent the radius of the interphase region and radius of the filler particle, respectively. The values  $E_f$ ,  $E_m$  and  $E_i$  denote the filler modulus, matrix modulus and interface modulus, and  $k$  is a factor that defines the ratio of interphase modulus to matrix modulus [34]. The minimum value of  $k$  is obtained when the interphase modulus is equal to matrix modulus (i.e. when

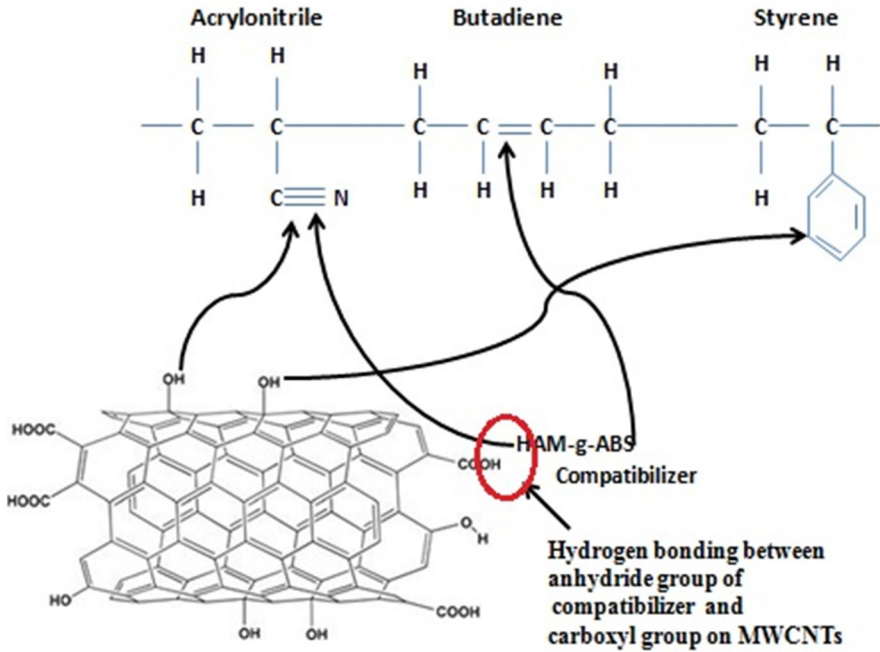
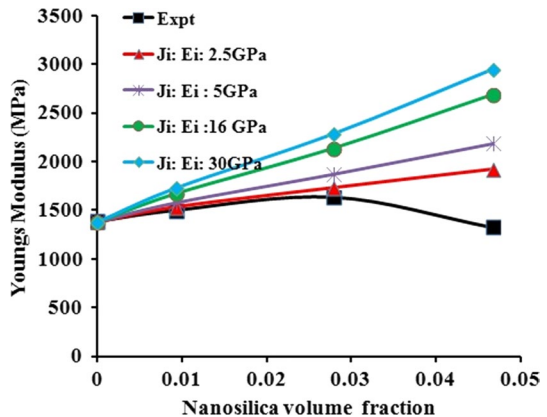


Fig. 5 Bonding mechanism of carboxyl-treated MWCNTs in the presence of ABS-g-MAH compatibilizer with comonomers of ABS matrix

$E_i = E_m$ ,  $k = 1$ ) while a maximum  $k$  value is reached when the interphase modulus is equal to the filler modulus (i.e.  $\max k = E_f/E_m$ ;  $k = 80/1.386 \text{ GPa} = 57.72$ ) [33]. Hence,  $k$  values can be varied from a minimum of 1 to a maximum  $E_f/E_m$  of 57.72. For each  $k$ , corresponding  $r_i$  could be estimated by fitting the experimental Young’s modulus values obtained for each composite with the Ji model. The average value of  $r_i$  obtained by this procedure is then used to estimate the interphase

Fig. 6 Young’s modulus of ABS/nanosilica-reinforced composites: experimental data and values estimated by the Ji model for various values of the interphase modulus  $E_i$



modulus ( $E_i$ ). Accordingly, the best agreement with experimental modulus values was reached for a  $r_i$  value of 105 nm and  $E_i$  of 2.5 GPa. Figure 6 shows the modulus prediction by Ji model as a function of nanosilica content at varying interphase modulus. It could be inferred that till 3 wt% of nanosilica content and at an interphase modulus of 2.5 GPa, the predicted modulus by Ji model is in well agreement and beyond 3 wt% modulus deviates from experimental and this could be due to nanosilica clustering.

In the case of MWCNT-reinforced ABS composites, the need to take into account also the aspect ratio of MWCNTs lead to the adoption of the Cox model as given by Eq. (2) [35–38].

$$E_C = (1 - v_f)E_m + n\eta_f v_f E_f \quad (2)$$

where

$$\eta_f = 1 - \frac{\tanh \beta}{\beta} \quad \text{and} \quad \beta = \frac{l}{d} \sqrt{\frac{-3E_m}{2E_f \ln v_f}} \quad (2(a), (b))$$

In these Eq. (2),  $E_f$  and  $E_m$  represent the modulus of filler and matrix, respectively. In these calculations,  $E_f$  of MWCNT was considered to be 450 GPa [2] and  $E_m$  is 1.386 GPa (obtained experimentally). The parameter  $v_f$  represents the volume fraction of the filler,  $(l/d)$  denotes the aspect ratio of MWCNT, and  $n$  defines the orientation of nanofiller in the matrix. In the case of randomly oriented fillers in the matrix,  $n$  can take a value of  $1/6$ , while  $n$  is  $1/2$  for the filler oriented in 2D plane and  $n$  is equal to 1 for a perfectly aligned reinforcement. The predictions of the Cox model are reported in Fig. 7 along with the experimental data.

The Cox model could satisfactorily predict the modulus of the MWCNT-reinforced ABS composites till 2 wt% of MWCNTs, while at higher filler content the deviation is most likely due to nanotube bundling and arise of aggregates.

Conclusively, the predictions demonstrate that filler aspect ratio, filler content, the interfacial properties, matrix and filler characteristics have a significant effect on the composite properties. The findings detailed that enhancement of mechanical

**Fig. 7** Young's modulus of ABS/MWCNT-reinforced composites: experimental data and values estimated by the Cox model for various values of aspect ratio of MWCNT

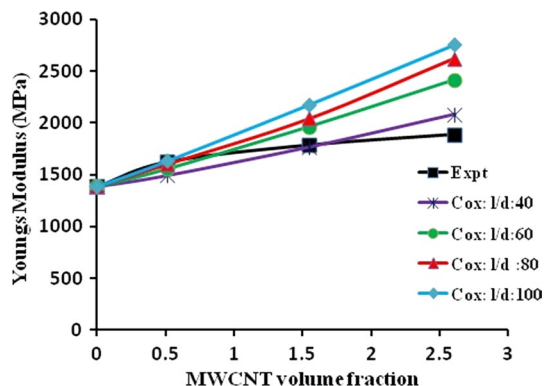
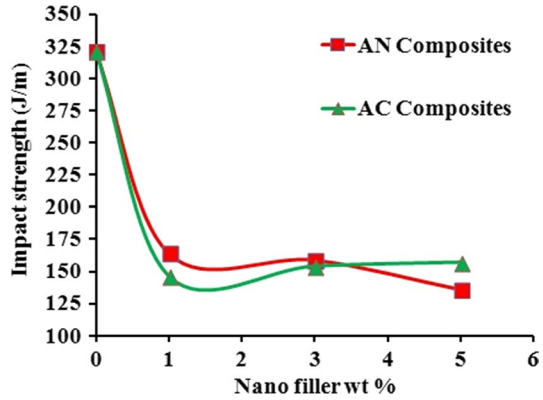


**Fig. 8** Impact strength as a function of nanosilica and CNT content



properties could be achieved desirably with good dispersion of fillers (as observed in micrographs in the present study) within the matrix which could reduce stress concentration zones and can lead to effective load transfer when high aspect ratio of fillers could be maintained during processing. Strong interfaces could transfer the stress from matrix to fillers, while generation of weak interfaces leads to stress concentration at nanofiller–matrix interface which causes failure of the composites.

### Impact strength

The differences in impact strength between composites obtained with the two different nanofillers are summarized in Fig. 8. Virgin ABS exhibits an impact strength of 321 J/m. In general, both NS and MWCNT have a negative effect on the impact strength of the ABS matrix. It could be observed that NS-reinforced composites exhibit higher impact strength in comparison with CNT-reinforced composites. At lower content of 1 and 3 wt% nanosilica, the impact strength of AN1 and AN3 composites is 164 and 159 J/m, respectively, which is higher than AC1 and AC3 composites. This shows the capability of nanosilica-reinforced composites to absorb more energy than CNT-reinforced composites and could withstand higher loading under external forces [39]. It is well accepted that cavitation and cavitation-induced shear yielding are the prominent mechanism of the toughening of particulate-filled polymers [40]. Cavitations at the boundary of the filler and in the polymer phase could trigger shear yielding in the ligament between the two voids. The weak interface developed in ABS nanosilica composites could impede the sudden stress transfer from the matrix to fillers and could absorb more energy and the crack takes more time to propagate through the composites. In the case of CNT-reinforced composites at 3 and 5 wt% of CNT content, impact strength values are 154 and 157 J/m, respectively. Even though the entanglement density and reinforcing efficiency would be higher in the case of MWCNT-reinforced composites, the prime factor that leads to the decrement in impact strength is due to the strong interfaces.

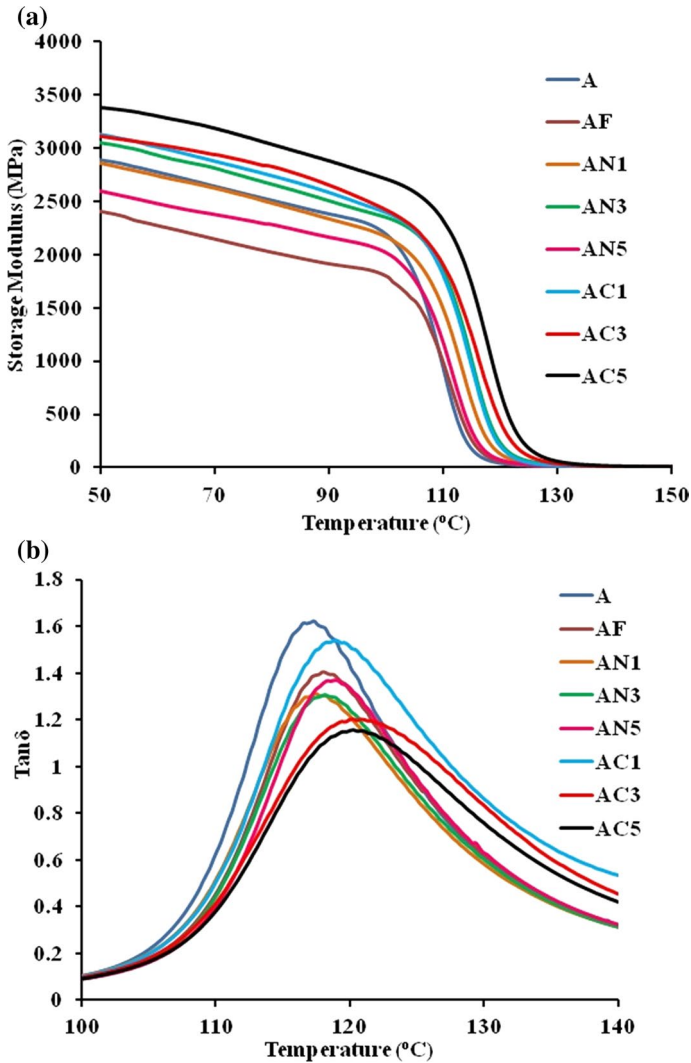


**Fig. 9** **a** The variation in storage modulus **b** variation in  $\tan\delta$  as a function of temperature

A strong interface may lead to abrupt stress transfer and brittle fracture upon an impact loading. Due to the high aspect ratio of CNTs, polymer chains can wrap around CNTs and could stretch and it exhibits a semi-ductile fracture relative to ductile behaviour of nanosilica composites. The impact strength values obtained for AC and AN composites could be mapped with the results obtained under static mechanical properties. The composite AC5 which exhibits highest tensile strength and brittle fracture experienced an obvious reduction in impact strength which indicates a decrement in toughness value by 2 units with regard to AN3 composite. At higher content of nanosilica (5 wt%), particle

agglomeration is intensified, and nanoclusters lead to sudden stress transfer and resulted in a drop in impact strength value.

## Dynamic mechanical analysis

The variation of storage modulus and  $\tan \delta$  as a function of temperature at a frequency of 1 Hz is plotted in Fig. 9a, b. The highest storage modulus was exhibited by AC5 composite followed by AC3 which delineates the stiffness of the material, energy stored and the elastic nature. As discussed already, the enhanced interfacial adhesion in the presence of carboxyl treated high aspect ratio CNTs led to an enhanced storage modulus in comparison with nanosilica-filled composites. As the temperature rises, near the glass transition region ( $T_g$ ) a drop in storage modulus could be noticed owing to the segmental mobility induced in the tight packed polymer chains [19, 41, 42]. The adherence, entanglement density and the reinforcing efficiency developed in CNT reinforced composites are particularly high in comparison with nanosilica-reinforced composites due to the high stiffening effect, geometrical aspects and high specific area of MWCNT. The effectiveness of filler dispersion and stress transfer is dominant in the presence of long curly nanotubes relative to silane-treated spherical 0D nanosilica.

The viscous and the elastic response of the composites could be analysed from the damping response of the composites. It is revealed that damping parameter goes through a maximum at the glass transition temperature and then decreased in rubbery region and also there is a decrement in  $\tan \delta$  as the weight content of filler increases. The significant right shift in  $T_g$  for AC3 and AC5 composites could be attributed to the constrained polymer chains when they entangle with long curly MWCNTs which generates immobilized regions which in turn lead to enhanced reinforcing efficiency and entanglement density. Furthermore, the lowered and the broadened peak of AC3 and AC5 indicate the improved interfacial adhesion and the higher number of restrained regions. These observations could be further correlated with the consistent dispersion of fillers and the enhanced mechanical properties.

The lowered and broadened  $\tan \delta$  of AN3 composite also shows the ability of the material to restrict the mobility of polymer chains upon deformation [43].

## Modelling of viscoelastic properties

### Prediction of Storage modulus

The storage modulus values experimentally obtained at the glassy plateau (50 °C), in the glass transition region (100 °C) and at the rubbery state (130 °C) are reported in Table 3.

An attempt has been made to model the storage modulus using different theoretical models.

**Table 3** Comparison of experimental and predicted storage modulus of nanosilica and carbon nanotube ABS composites from glassy plateau to rubbery region

Specimen	Storage modulus (MPa) Experimental			Storage modulus (MPa) Einstein model			Storage modulus (MPa) Guth model			Storage modulus (MPa) Mooney model		
	50 °C	100 °C	130 °C	50 °C	100 °C	130 °C	50 °C	100 °C	130 °C	50 °C	100 °C	130 °C
A	2895.6	2185.9	12.15	2895.6	2185.98	12.15	2895.6	2185.9	12.15	2895.6	2185.9	12.15
AN1	2855.2	2161.6	22.42	2922.5	2206.3	12.26	2966.5	2239	12.4	2964.2	2237.8	12.44
AN3	3045.6	2345.2	29.04	2976.4	2246.9	12.48	3129	2362	13.13	3111	2348.6	13.1
AN5	2599.7	2022.8	16.9	3030.8	2288	12.7	3322.7	2508	13.94	3272.8	2470.8	13.73
AC1	3123.9	2389.6	18.36	2910.4	2197	12.2	2933.6	2214	12.3	2932.9	2214.2	12.31
AC3	3116.8	2422.7	37.48	2940.5	2219.8	12.3	3017.6	2278	12.6	3011.9	2273	12.6
AC5	3387.6	2712.4	59.57	2971.2	2243.03	12.5	3112.2	2349.6	13.06	3096	2337	12.9

Einstein proposed a theoretical model for the prediction of modulus which is correlated with filler fraction incorporated in the ABS base matrix. Einstein model [44–46] is represented by Eq. (3)

$$G_C = G_m(1 + v_f) \tag{3}$$

where  $G_C$  and  $G_m$  denote the storage modulus of composite and matrix, respectively, and  $v_f$  is the volume fraction of fillers. Guth [19, 44, 47, 48] modified the Einstein’s equation as follows:

$$G_C = G_m \left( 1 + 2.5 v_f + 14.1 v_f^2 \right) \tag{4}$$

An exponential relation was proposed by Mooney [44] which takes into account the relative sedimentation volume of the inclusion (crowding factor, S) and is defined as the ratio of apparent to the true volume occupied by the filler inclusions. Mooney’s model is expressed by Eq. (5).

$$G_C = G_m \exp \left( \frac{2.5 v_f}{1 - S v_f} \right) \tag{5}$$

The experimental and the theoretical storage moduli of the nanosilica and CNT-based ABS composites at different filler loadings are reported in Table 3. Einstein model agrees with experimental values, while Guth and Mooney models show slight deviation from experimental results but could be considered to be satisfactory in predicting the composite behaviour.

In the case of Einstein’s model, it could be observed that at low loadings of nanosilica (1 and 3 wt%) deviation from glassy plateau to glass transition region is in the range of 2 to 4% with respect to experimental modulus. At higher content of nanosilica (5 wt%), Einstein’s model predictions deviate up to 16%. On the other hand, Einstein’s predictions for CNT-reinforced composites at low loadings (1 and 3 wt%) deviate from 5 to 8% till glass transition and at higher loadings (5 wt%) deviation is up to 17%. Guth and Mooney model also agrees well with experimental values and could satisfactorily predict the composite behaviour. At higher content (5 wt%) of spherical nanosilica particles, Mooney and Guth models deviate from 22 to 27% (till  $T_g$ ) and is higher in comparison with Einstein’s model. At higher loadings of

**Table 4** Comparison of experimental and best predicted storage modulus values at glass transition region

Specimen	Storage modulus (MPa)	Best agreeing theoretical values	% deviation experimental value
AN1	2161.6	2206.3 (Einstein’s model); 2239.5 (Guth’s model)	2.06, 3.6
AN3	2345	2246.9 (Einstein’s model), 2362 (Guth’s model)	4.1, 0.73
AN5	2022.8	2288 (Einstein’s model)	13
AC1	2389.6	2214.6 (Guth’s model); 2214 (Mooney model)	7.3; 7.3
AC3	2422.77	2278.1 (Guth’s model); 2273.85 (Mooney model)	5.9; 6.1
AC5	2712.38	2349.6 (Guth’s model); 2337.47 (Mooney model)	13.3; 13.8

CNT, Mooney and Guth deviates from 8 to 13% from glassy plateau to  $T_g$  region. It could be inferred that at higher contents of nanosilica percentage deviation of storage modulus predicted by all the models from the experimental results are larger in comparison with CNT-reinforced ABS composites. Another inference could be that at 5 wt% CNT reinforcement Guth and Mooney model agrees the best with regard to Einstein's model. In addition at 5 wt% nanosilica reinforcements, Einstein model agrees the best relative to Mooney and Guth's predictions. The best theoretical model predictions are reported in Table 4.

Cohan [49] modified Guth's equation by incorporating aspect ratio ( $\rho$ ) in the model and the proposed equation is of the form.

$$G_C = G_m \left( 1 + 0.675 \rho + 1.62 \rho^2 v_f + 14.1 v_f^2 \right) \quad (6)$$

This model deviates largely from experimental results owing to the parameter  $\rho$  in the equation. Introducing an aspect ratio of 80 in Cohan's model will result in very high values of storage modulus relative to other models.

### Modelling of damping behaviour

Rigid filler inclusions decrease the damping behaviour of the composites as suggested by Nielsen's classical rule of mixtures. Nielsen's model [49–51] can be expressed by Eq. (7).

$$\tan \delta_{Composite} = v_{filler} \tan \delta_{filler} + v_{matrix} \tan \delta_{matrix} \quad (7)$$

Since rigid fillers offer very low damping (i.e.  $\tan \delta_{filler} \approx 0$ ), and hence, the first term in Eq. (7) could be eliminated. Therefore, Eq. (7) reduces to:

$$\tan \delta_{Composite} = v_{matrix} \tan \delta_{matrix} \quad (8)$$

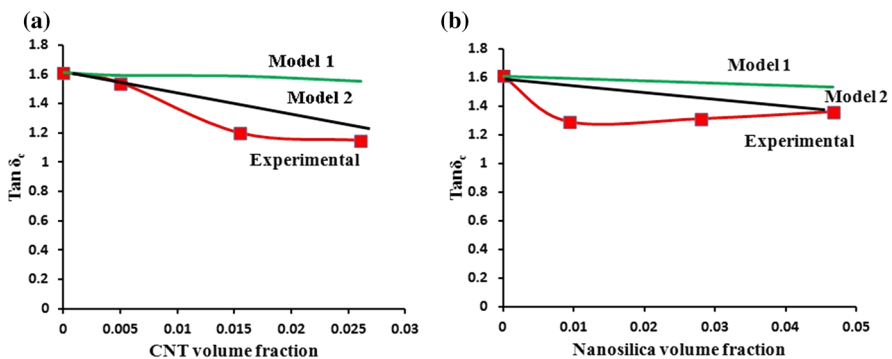


**Fig. 10** Comparison of experimental and theoretical modelling of damping values as a function of **a** volume fraction of CNT-reinforced ABS composites **b** volume fraction of nanosilica-reinforced ABS composites

and the damping is controlled by matrix. The interactions of inclusions with the matrix could offer some additional constraints which in turn can further cause a decrement in damping values. Hence, a stiffness factor [49] is incorporated in the above model and Eq. (8) can be rewritten as (9).

$$\tan \delta_{Composite} = (1 - v_{filler}) \left( \frac{E_{matrix}}{E_{Composite}} \right) \tan \delta_{matrix} \tag{9}$$

It is assumed that the matrix in the presence of fillers offers a stiffness equivalent to the minimum elastic modulus of the composite [52]. In the region of glass transition, the extent of mobility of polymer chains is high and damping is completely dependent on matrix phase as expressed in Eq. (9). In Fig. 10a, b, the experimental and the predicted damping values are plotted as a function of volume fraction of nanosilica and MWCNT. It could be observed that Model 2 is in close agreement with experimental damping values in the case of MWCNT reinforced composites. At 3 wt%, MWCNT loading experimental damping values are the minimum which shows that entanglement density of polymer chains is maximum at this optimum filler content. The damping value at 5 wt% MWCNT is not much deviating from 3 wt% MWCNT which explains the possibility of better entanglement even at 5 wt% MWCNTs. Like experimental results, Model 2 also shows a decreasing trend of damping parameter with increase in CNT filler content. Model 2 predicts the damping behaviour well due to the fact that restraints imposed due to entanglement of polymer chains in existence with high aspect ratio CNTs are taken into account by this model since stiffness factor is incorporated. On the other hand, for nanosilica-reinforced composites experimentally damping parameter reached the lowest values at 1 wt% and 3 wt% where the possibility of entanglement density would be higher. At higher content of 5 wt% nanosilica loading, an increase in damping is noted owing to the impedance proffered to the possible entanglements as a result of agglomerations. Model 2 approximates with experimental behaviour of nanosilica composites, but the percentage deviations from experimental results are slightly higher with respect to MWCNT-reinforced composites and this could be due to the differences in the reinforcing efficiency of two geometrically different fillers.

**Fig. 11** Solvent absorption curve of ABS-reinforced MWCNT composites

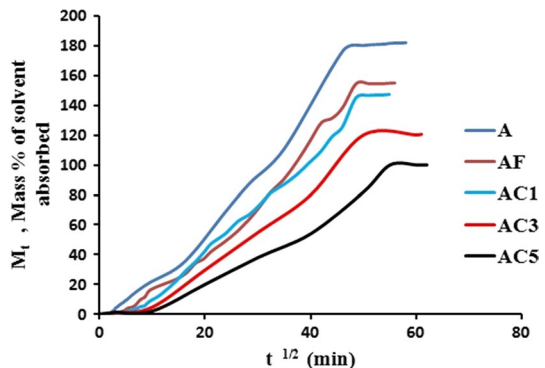


**Fig. 12** Solvent absorption curve of ABS/nanosilica-reinforced composites

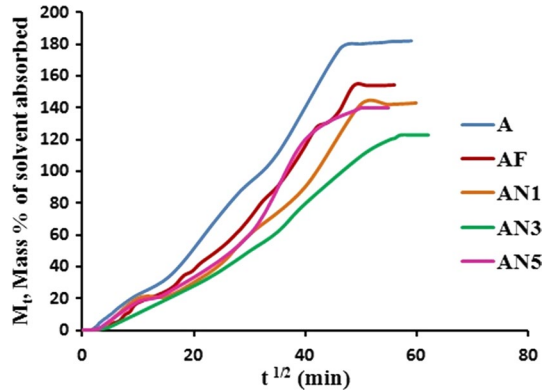


**Table 5** Transport properties of virgin ABS, MWCNT/nanosilica reinforced composites

Sample	Diffusivity *10 <sup>-10</sup> (m <sup>2</sup> /s)	Sorption coefficient	Permeability*10 <sup>-10</sup> (m <sup>2</sup> /s)
A	0.0819	2.83	0.231
AF	0.0732	2.54	0.186
AC1	0.0588	2.46	0.145
AC3	0.0582	2.29	0.133
AC5	0.0400	2.18	0.087
AN1	0.1997	2.32	0.147
AN3	0.0667	2.27	0.151
AN5	0.0969	2.19	0.212

Predictions of Model 1 deviate from experimental results more than those of model 2 because this approach avoids the effect of localized constraints played by both fillers on matrix deformation.

## Transport behaviour

The barrier properties are of interest in polymer composites when they are used for packaging applications. It is important to assess the rate of diffusion of solvent within the composite once it progresses from high concentration to low concentration. The diffusion behaviour can be classified mathematically from the shape of the initial part of the absorption curve. The solvent uptake can be represented by Eq. (10)

$$M_t = kt^n \quad (10)$$

where  $t$  is the time and  $k$  is the initial slope of the  $M_t$  versus  $\sqrt{t}$  curve and  $n$  is a constant, where for the Fickian absorption  $n=0.5$ , while the non-Fickian absorption

is characterized by  $0.5 < n < 1$  [53]. The mass percentage of solvent sorbed can be determined using Eq. (11):

$$M_t = \frac{W_t - W_0}{W_0} \times 100 \tag{11}$$

where  $W_t$  denotes the mass of the solvent sorbed at a given time  $t$ , and  $W_0$  is the initial mass of the dry samples. Sorption studies were conducted on neat ABS (A) and composites at room temperature using toluene as a solvent. Figures 11 and 12 represent the solvent uptake of the composites with time (master curve) with a linearly increasing trend during the initial time period of the sorption studies and at the later stages a saturated plateau of solvent uptake could be observed. The transport properties like permeability, diffusivity and sorption coefficient are reported in Table 5 which could be estimated from the dimensions of the sorption test samples and from the master curve data. The sorption coefficient was estimated using the expression of Eq. (12) [54].

$$S = \frac{W_\alpha}{W_s} \tag{12}$$

where  $W_\alpha$  is the mass of the solvent absorbed which was quantified at the state of equilibrium swelling of the composite samples and  $W_s$  denotes the initial weight of the samples. The diffusivity ( $D$ ) of toluene solvent through the composite samples could be evaluated using the diffusion coefficient given by the Fick's law (13) [55].

$$D = \pi \left( \frac{h\theta}{4M_\infty} \right)^2 \tag{13}$$

$M_\alpha$  is the mass percentage of the solvent uptake at the state of equilibrium swelling,  $h$  is the thickness of the sample and  $\theta$  is the slope of the initial portion of the absorption curve. Furthermore, permeability could be computed as the product of diffusivity ( $D$ ) and the sorption coefficient ( $S$ ) as in Eq. (14) [43].

$$P = S \times D \tag{14}$$

Amongst the MWCNT-reinforced composites, AC5 offers the lowest diffusivity and permeability with regard to other composites. The diffusion coefficient decremented by 51% and permeability decreased by 62% with respect to neat ABS.

The reason for the decrease in diffusivity is the reduction in free volume with the incorporation of fillers. The better dispersion and the interfacial adhesion (confirmed from the SEM and TEM images) between the filler and the matrix also attribute to the decrement in the diffusivity. The secondary interaction between the styrene part on ABS and  $\pi$  electronic network of MWCNTs surface forms a rigid phase and polymer chains could strongly wrap on these rigid phase. In nanosilica-reinforced composites, AN3 composites exhibited drop in diffusivity and permeability by 18.5% and 34.6%, respectively, in comparison with ABS.

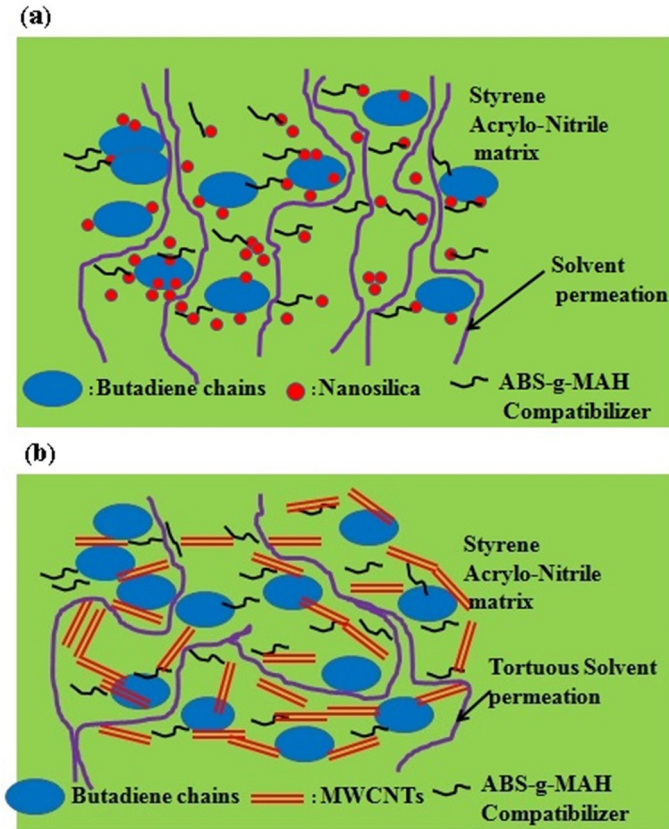


**Fig. 13** Illustration of solvent permeation through **a** nanosilica reinforced **b** MWCNT

In the case of nanosilica particles, 0D spherical shape, and the increase in free volume in the matrix phase are the factors for the enhanced permeation of solvent with respect to MWCNTs.

The higher aspect ratios of MWCNTs could lead to more tortuous path of permeant solvent than spherical shape reinforcements as presented in Fig. 13. Additionally, the solvent molecules take up more time to penetrate through the composite structure packed with entangled network of MWCNTs with ABS chains.

## Conclusions

The following conclusions are drawn from this work on nanosilica and MWCNT-reinforced acrylonitrile–butadiene–styrene composites.

- From the TEM images, it was found that an excellent dispersion of fillers occurred within the matrix at 5 wt% of CNT content. It could also be inferred that while comparing the TEM images of nanosilica and MWCNT reinforced composites, the dispersion achieved in carboxylic acid-treated MWCNT composites was prominent than silane-treated nanosilica ABS composites.
- The enhancement in tensile strength was maximum for the composite at 5wt% MWCNT content. The decrement in modulus and tensile strength beyond 3 wt% of nanosilica was due to the generation of agglomerates. The Young's modulus of nanosilica reinforced composites was predicted by Ji model, and it was estimated that at an interphase modulus of 2.5 GPa and interface radius of 105 nm, the modulus obtained was close to experimental modulus till 3 wt% filler content. In the case of MWCNT composites, Cox model was the most suitable to model the modulus at different aspect ratios and at an aspect ratio of 80 (average  $l/d$  confirmed from TEM images), experimental modulus was in well agreement with theoretical modulus.
- The elongation at break for ABS/nanosilica composites at 3 wt% was higher in comparison with ABS/CNT composites which indicate the semi-ductile behaviour of nanosilica composites with regard to the brittle nature of CNT-reinforced composites as manifested by strain at break values.
- The highest storage modulus was obtained for AC5 composites which can be attributed to the enhanced interfacial adhesion in the presence of carboxyl treated high aspect ratio CNTs. The estimated damping parameter and the lowered and the broadened peak achieved by AC3, AC5 and AN3 composites revealed the possibility of higher number of constrained phases and strong interfacial adhesion.
- The prediction of storage modulus was performed using theoretical models. The damping parameters estimated using theoretical model 2 which takes into account the stiffness parameter showed a decreasing trend in damping parameter which verified the constrictions imposed by the fillers. The CNT-reinforced composite system indicated a best fit with model 2 which delineated the possibility of higher entanglement density with high aspect ratio MWCNTs.
- The diffusion coefficient decreased by 51% for AC5 composite with respect to neat ABS, whereas AN3 composite demonstrated a decrement in diffusivity by 18.5%. The free volume available, better dispersion of high aspect ratio MWCNTs, interfacial adhesion and higher degree of entanglement provide a tortuous path for the permeation of solvent through the composite.

**Acknowledgements** The authors thank Sophisticated Testing and Instrumentation Centre (STIC), Kochi, India, for TEM analysis. The authors are grateful to Centre of excellence in Advanced Materials and Green Technologies (CoE-AMGT) Amrita School of Engineering, Coimbatore, Amrita Vishwa Vidyapeetham, India, for SEM analysis.

**Funding** This research did not receive any specific grant from funding agencies in the public, commercial or not-for-profit sectors.

## Declarations

**Conflicts of interest** None declared.

## References

1. Kumar V, Ramkumar J, Aravindan S et al (2009) Fabrication and characterization of ABS nano composite reinforced by nano sized alumina particulates. *Int J Plast Technol* 13:133–149. <https://doi.org/10.1007/s12588-009-0011-5>
2. Al-Saleh MH, Al-Saidi BA, Al-Zoubi RM (2016) Experimental and theoretical analysis of the mechanical and thermal properties of carbon nanotube/acrylonitrile–styrene–butadiene nanocomposites. *Polym* 89:12–17. <https://doi.org/10.1016/j.polymer.2016.01.053>
3. Abedini A, Asiyabi T, Campbell HR et al (2019) On fabrication and characteristics of injection molded ABS/Al<sub>2</sub>O<sub>3</sub> nanocomposites. *Int J Adv Manf Technol* 102:1747–1758
4. Rasana N, Jayanarayanan K (2019) Experimental and micromechanical modeling of fracture toughness: MWCNT-reinforced polypropylene/glass fiber hybrid composites. *J Thermoplast Compos Mater* 32:1031–1055. <https://doi.org/10.1177/0892705718785687>
5. Liang W, Duan Z, Kuo S et al (2018) Mechanical performance of nano-Al<sub>2</sub>O<sub>3</sub>-modified composites at cryogenic and room temperatures. *Polym Compos* 39:3006–3012
6. Chandra A, Turng LS, Ke Li et al (2011) Fracture behavior and optical properties of melt compounded semi-transparent polycarbonate (PC)/alumina nanocomposites. *Compos Part A: Appl Sci Manuf* 42:1903–1909. <https://doi.org/10.1016/j.compositesa.2011.08.015>
7. Yu W, Xie H, Chen L et al (2017) Synergistic thermal conductivity enhancement of PC/ABS composites containing alumina/magnesia/graphene nanoplatelets. *Polym Compos* 38:2221–2227
8. Zakaria MR, Akil HM, Kudus MH et al (2014) Enhancement of tensile and thermal properties of epoxy nanocomposites through chemical hybridization of carbon nanotubes and alumina. *Compos Part A: Appl Sci Manuf* 66:109–116. <https://doi.org/10.1016/j.compositesa.2014.07.008>
9. Lin Y, Chen Y, Zeng Z et al (2015) Effect of ZnO nanoparticles doped graphene on static and dynamic mechanical properties of natural rubber composites. *Compos Part A: Appl Sci Manuf* 70:35–44. <https://doi.org/10.1016/j.compositesa.2014.12.008>
10. Hammani S, Barhoum A, Bechelany M (2018) Fabrication of PMMA/ZnO nanocomposite: effect of high nanoparticles loading on the optical and thermal properties. *J Mater Sci* 53:1911–1921. <https://doi.org/10.1007/s10853-017-1654-9>
11. Shofner ML, Rodríguez-Macías FJ, Vaidyanathan R et al (2003) Single wall nanotube and vapor grown carbon fiber reinforced polymers processed by extrusion freeform fabrication. *Compos Part A: Appl Sci Manuf* 34:1207–1217. <https://doi.org/10.1016/j.compositesa.2003.07.002>
12. Khan AN, Waheed Q, Jan R et al (2018) Experimental and theoretical correlation of reinforcement trends in acrylonitrile butadiene styrene/single-walled carbon nanotubes hybrid composites. *Polym Compos* 39(S2):E902–E908. <https://doi.org/10.1002/pc.24321>
13. Jouyandeh M, Karami Z, Jazani OM et al (2019) Curing epoxy resin with anhydride in the presence of halloysite nanotubes: the contradictory effects of filler concentration. *Prog Org Coat* 126:129–135. <https://doi.org/10.1016/j.porgcoat.2018.10.007>
14. Kotal M, Bhowmick AK (2015) Polymer nanocomposites from modified clays: Recent advances and challenges. *Prog Polym Sci* 51:127–187. <https://doi.org/10.1016/j.progpolymsci.2015.10.001>
15. Jenifer A, Rasana N, Jayanarayanan K (2018) Synergistic effect of the inclusion of glass fibers and halloysite nanotubes on the static and dynamic mechanical, thermal and flame retardant properties of polypropylene. *Mater Res Express* 5:065308. <https://doi.org/10.1088/2053-1591/aac67d>
16. Pedrazzoli D, Pegoretti A (2014) Hybridization of short glass fiber polypropylene composites with nanosilica and graphite nanoplatelets. *J Reinf Plast and Comp* 33:1682–1695. <https://doi.org/10.1177/0731684414542668>

17. Gao A, Zhao F, Wang F et al (2019) Highly conductive and light-weight acrylonitrile-butadiene-styrene copolymer/reduced graphene nanocomposites with segregated conductive structure. *Compos Part A: Appl Sci Manuf* 122:1–7. <https://doi.org/10.1016/j.compositesa.2019.04.019>
18. Yamamoto BE, Trimble AZ, Minei B et al (2019) Development of multifunctional nanocomposites with 3-D printing additive manufacturing and low graphene loading. *J Thermoplast Compos Mater* 32:383–408. <https://doi.org/10.1177/0892705718759390>
19. Abraham J, Thomas J, Kalarikkal N et al (2018) Static and dynamic mechanical characteristics of ionic liquid modified MWCNT-SBR composites: theoretical perspectives for the nanoscale reinforcement mechanism. *J Phys Chem B* 122:1525–1536. <https://doi.org/10.1021/acs.jpcc.7b10479>
20. Schmitz DP, Silva TI, Ramoa SD et al (2018) Hybrid composites of ABS with carbonaceous fillers for electromagnetic shielding applications. *J Appl Polym Sci* 135:46546. <https://doi.org/10.1002/app.46546>
21. Kyratsis P, Tzetzis D (2018) Investigation of the mechanical properties of acrylonitrile butadiene styrene (ABS)-nanosilica reinforced nanocomposites for fused filament fabrication 3D printing. In *IOP Conf Series: Mater Sci Eng* 416:012086. <https://doi.org/10.1088/1757-899X/416/1/012086>
22. Xiao MZ, Wang YZ, Yeh JT (2014) Properties of Recycled ABS Modified with Nanosilica. *Chin J Coll Poly* 2014:03
23. Rostamiyan Y, Bakhshi A (2019) Study on Compression and Flexural Behavior of ABS-SiO<sub>2</sub> Polymer Matrix Composite Fabricated by Hot Extrusion. *Mech Adv Compos Struct* 6:239–247
24. Jyoti J, Basu S, Singh BP, Dhakate SR (2015) Superior mechanical and electrical properties of multiwall carbon nanotube reinforced acrylonitrile butadiene styrene high performance composites. *Compos Part B: Eng* 83:58–65. <https://doi.org/10.1016/j.compositesb.2015.08.055>
25. Jyoti J, Singh BP, Arya AK et al (2016) Dynamic mechanical properties of multiwall carbon nanotube reinforced ABS composites and their correlation with entanglement density, adhesion, and reinforcement and C factor. *RSC Adv* 6:3997–4006. <https://doi.org/10.1039/c5ra25561a>
26. Al-Saleh MH, Al-Anid HK, Husain YA et al (2013) Impedance characteristics and conductivity of CNT/ABS nanocomposites. *J Phys D: Appl Phys* 46:385305. <https://doi.org/10.1088/0022-3727/46/38/385305>
27. Dul S, Fambri L, Pegoretti A (2018) Filaments production and fused deposition modelling of ABS/carbon nanotubes composites. *Nanomaterials* 8:49. <https://doi.org/10.3390/nano8010049>
28. Kapoor S, Goyal M, Jindal P (2017) Effect of multi-walled carbon nanotubes (MWCNT) on mechanical properties of acrylonitrile butadiene styrene (ABS) nano-composite. *Indian J Sci Technol* 10(17):1–6
29. Gardea F, Cole DP, Glaz B, Riddick JC (2019) Energy dissipation characteristics of additively manufactured CNT/ABS nanocomposites. *Rapid Prototyp J*. <https://doi.org/10.1108/RPJ-08-2018-0204>
30. Lin OH, Akil HM, Mohd Ishak ZA (2011) Surface-activated nanosilica treated with silane coupling agents/polypropylene composites: mechanical, morphological, and thermal studies. *Polym Compos* 32:1568–1583. <https://doi.org/10.1002/pc.21190>
31. Wang R, Kuan HC, Qiu A et al (2020) A facile approach to the scalable preparation of thermoplastic/carbon nanotube composites. *Nanotechnology* 31:195706. <https://doi.org/10.1088/1361-6528/ab5a28>
32. Yonghong D, Jinghong Y, Liang G (2019) Surface carboxylation of multi-walled carbon nanotubes and its properties of flame retardant ABS. *Eng Plast Appl* 47:1–6
33. Zare Y (2015) Assumption of interphase properties in classical Christensen–Lo model for Young’s modulus of polymer nanocomposites reinforced with spherical nanoparticles. *RSC Adv* 5:95532–95538. <https://doi.org/10.1039/c5ra19330c>
34. Ji XL, Jing JK, Jiang W et al (2002) Tensile modulus of polymer nanocomposites. *Polym Eng Sci* 42:983–993. <https://doi.org/10.1002/pen.11007>
35. Cox HL (1952) The elasticity and strength of paper and other fibrous materials. *Br J Appl Phys*. <https://doi.org/10.1088/0508-3443/3/3/302>
36. Coleman JN, Khan U, Blau WJ et al (2006) Small but strong: a review of the mechanical properties of carbon nanotube–polymer composites. *Carbon* 44:1624–1652. <https://doi.org/10.1016/j.carbon.2006.02.038>
37. Lee KY, Aitomäki Y, Berglund LA et al (2014) On the use of nanocellulose as reinforcement in polymer matrix composites. *Compos Sci Technol* 105:15–27. <https://doi.org/10.1016/j.compscitech.2014.08.032>

38. Taha I, Abdin YF (2011) Modeling of strength and stiffness of short randomly oriented glass fiber—polypropylene composites. *J Compos Mater* 45:1805–1821. <https://doi.org/10.1177/0021998310389089>
39. Jiang L, Lam YC, Tam KC et al (2005) Strengthening acrylonitrile-butadiene-styrene (ABS) with nano-sized and micron-sized calcium carbonate. *Polymer* 46:243–252. <https://doi.org/10.1016/j.polymer.2004.11.001>
40. Carolan D, Ivankovic A, Kinloch AJ et al (2017) Toughened carbon fibre-reinforced polymer composites with nanoparticle-modified epoxy matrices. *J Mater Sci* 52:1767–1788. <https://doi.org/10.1007/s10853-016-0468-5>
41. Arivazhagan A, Masood SH (2012) Dynamic mechanical properties of ABS material processed by fused deposition modelling. *Int J Eng Res Appl* 2:2009–2014
42. Pandey AK, Kumar R, Kachhava VS et al (2016) Mechanical and thermal behaviours of graphite flake-reinforced acrylonitrile–butadiene–styrene composites and their correlation with entanglement density, adhesion, reinforcement and C factor. *RSC Adv* 6:50559–50571. <https://doi.org/10.1039/C6RA09236E>
43. Rasana N, Jayanarayanan K (2018) Polypropylene/short glass fiber/nanosilica hybrid composites: evaluation of morphology, mechanical, thermal, and transport properties. *Polym Bull* 75:2587–2605. <https://doi.org/10.1007/s00289-017-2173-1>
44. Joseph PV, Mathew G, Joseph K et al (2003) Dynamic mechanical properties of short sisal fibre reinforced polypropylene composites. *Compos Part A: Appl Sci Manuf* 34:275–290. [https://doi.org/10.1016/S1359-835X\(02\)00020-9](https://doi.org/10.1016/S1359-835X(02)00020-9)
45. Kajohnchaiyagual J, Jubsilp C, Dueramae I et al (2014) Thermal and mechanical properties enhancement obtained in highly filled alumina-polybenzoxazine composites. *Polym Compos* 35:2269–2279. <https://doi.org/10.1002/pc.22892>
46. Ashok N, Balachandran M, Das NC et al (2021) Nanoreinforcement mechanism of organomodified layered silicates in EPDM/CIIR blends: experimental analysis and theoretical perspectives of static mechanical and viscoelastic behavior. *Compos Inter* 28:35–62. <https://doi.org/10.1080/09276440.2020.1736879>
47. Praveen S, Chattopadhyay PK, Albert PA et al (2009) Synergistic effect of carbon black and nano-clay fillers in styrene butadiene rubber matrix: development of dual structure. *Compos Part A: Appl Sci Manuf* 40:309–316. <https://doi.org/10.1016/j.compositesa.2008.12.008>
48. Elhaouzi F, Nourdine A, Brosseau C et al (2019) Hyperelastic behavior and dynamic mechanical relaxation in carbon black-polymer composites. *Polym Compos* 40:3005–3011. <https://doi.org/10.1002/pc.25142>
49. Jayanarayanan K, Rasana N, Mishra RK (2017) Dynamic mechanical thermal analysis of polymer nanocomposites. In *Thermal and rheological measurement techniques for nanomaterials characterization*. Elsevier 2017:123–157. <https://doi.org/10.1016/B978-0-323-46139-9.00006-2>
50. Jayanarayanan K, Thomas S, Joseph K (2016) Effect of blend ratio on the dynamic mechanical and thermal degradation behavior of polymer–polymer composites from low density polyethylene and polyethylene terephthalate. *Iran Polym J* 25:373–384. <https://doi.org/10.1007/s13726-016-0429-5>
51. Tahreen N, Masud AK (2012) Investigation of the mechanical properties of polyethylene/carbon nanotube composite by molecular dynamics simulation. *Int J Nano Biomater* 4:54–68. <https://doi.org/10.1504/IJNB.2012.048217>
52. Idicula M, Malhotra SK, Joseph K et al (2005) Dynamic mechanical analysis of randomly oriented intimately mixed short banana/sisal hybrid fibre reinforced polyester composites. *Compos Sci Technol* 65:1077–1087. <https://doi.org/10.1016/j.compscitech.2004.10.023>
53. Verma D, Goh KL (2019) Natural fiber-reinforced polymer composites: application in marine environments. In *Biomass, Biopolymer-Based Materials, and Bioenergy* Woodhead Publishing. <https://doi.org/10.1016/B978-0-08-102426-3.00003-5>
54. Dhakal HN, MacMullen J, Zhang ZY (2016) Moisture measurement and effects on properties of marine composites. In *Marine Applications of Advanced Fibre-Reinforced Composites* Woodhead Publishing. <https://doi.org/10.1016/B978-1-78242-250-1.00005-3>
55. Abraham J, Maria HJ, George SC et al (2015) Transport characteristics of organic solvents through carbon nanotube filled styrene butadiene rubber nanocomposites: the influence of rubber–filler interaction, the degree of reinforcement and morphology. *Phys Chem Chem Phys* 17:11217–11228. <https://doi.org/10.1039/c5cp00719d>

**Publisher's Note** Springer Nature remains neutral with regard to jurisdictional claims in published maps and institutional affiliations.

## Authors and Affiliations

**N. Rasana**<sup>1,2</sup>  · **K. Jayanarayanan**<sup>1,2</sup>  · **Alessandro Pegoretti**<sup>3</sup>  ·  
**G. Rammanoj**<sup>1</sup> · **K. Arunkumar**<sup>1</sup> · **T. Hariprasanth**<sup>1</sup>

<sup>1</sup> Department of Chemical Engineering and Materials Science, Amrita School of Engineering - Coimbatore, Amrita Vishwa Vidyapeetham, Coimbatore 641 112, India

<sup>2</sup> Centre of Excellence in Advanced Materials and Green Technologies, Amrita Vishwa Vidyapeetham, Coimbatore 641 112, India

<sup>3</sup> Department of Industrial Engineering, University of Trento, Via Sommarive 9, 38123 Trento, Italy